

# Powder metallurgy routes toward aluminum boron nitride nanotube composites, their morphologies, structures and mechanical properties

Maho Yamaguchi<sup>a,b</sup>, Fanqiang Meng<sup>c</sup>, Konstantin Firestein<sup>d</sup>, Koichi Tsuchiya<sup>b,c</sup>,  
Dmitri Golberg<sup>a,b,\*</sup>

<sup>a</sup> Nanotube Unit, World Premier International Center for Materials Nanoarchitectonics (WPI-MANA), National Institute for Materials Science, Namiki 1-1, Tsukuba, Ibaraki 3050044, Japan

<sup>b</sup> Graduate School of Pure and Applied Sciences, University of Tsukuba, Tennodai 1, Tsukuba, Ibaraki 3050005, Japan

<sup>c</sup> Research Center for Strategic Materials, National Institute for Materials Science, 1-2-1 Sengen, Tsukuba, Ibaraki 3050044, Japan

<sup>d</sup> Laboratory of Inorganic Nanomaterials, National University of Science and Technology "MISIS", Leninsky pr. 4, Moscow 119049, Russian Federation

## ARTICLE INFO

### Article history:

Received 10 January 2014

Received in revised form

25 February 2014

Accepted 27 February 2014

Available online 12 March 2014

### Keywords:

Aluminum

Boron nitride nanotubes

Composite

Spark plasma sintering

High-pressure torsion

## ABSTRACT

Aluminum/boron nitride nanotube (BNNT) composites with up to 5 wt% (i.e., 9.7 vol%) nanotube fractions were prepared via spark plasma sintering (SPS) and high-pressure torsion (HPT) methods. Various microscopy techniques, X-ray diffraction, and energy dispersive X-ray analysis confirmed the integration of the two phases into decently dense and compact composites. No other phases, like Al borides or nitrides, formed in the Al–BNNTs macrocomposites of the two series. The BNNTs were found to be preferentially located along Al grain boundaries in SPS samples (grain size was 10–20 μm) creating micro-discontinuities and pores which were found to be detrimental for the sample hardness, whereas in HPT samples, the tubes were rather evenly distributed within a fine-grained Al matrix (grain size of several hundred nm). Therefore, the hardness of HPT samples was drastically increased with increasing BNNTs content in Al pellets. The value for Al–BNNT 3.0 wt% sample was more than doubled (190 MPa) compared to a pure Al–HPT compact (90 MPa). And the room temperature ultimate tensile strength of Al–BNNTs HPT samples containing 3.0 wt% BNNT (~300 MPa) became ~1.5 times larger than that of a BNNT-free HPT–Al compact (~200 MPa).

© 2014 Elsevier B.V. All rights reserved.

## 1. Introduction

Light metal matrix composites (MMCs) reinforced with nano-phases became a popular direction in Materials Science of the 21st century. To date, as a strengthening nanophase, most typically, carbon nanotubes (CNT) have been used. Most of the MMC–CNT composites have been produced by powder metallurgy techniques, such as mechanical alloying, sintering, hot pressing and compacting [1]. To do so, after the initial mixing step, a blend of CNTs and a metal must be consolidated to a high density. A wide range of compaction processes has been applied to reach a sufficient densification, among those spark plasma sintering (SPS) and high-pressure torsion (HPT) are particularly notable. SPS was used for the CNT–MMC studies (mostly for Al [2] and Cu–CNT systems [3,4]). For example, Kwon et al. [5] and Kurita et al. [6] found that CNTs may be well dispersed within an Al matrix by using a hetero-agglomeration principle. And 5.0 vol% CNTs addition could elevate

the strength to about thrice of that of pure Al [5]. This improvement was attributed to particular strengthening by CNTs, which are strongly bonded with the matrix through the crystallized Al carbide phase [5]. A fully dense 1.0 vol% MWCNT–Al matrix composite has documented a 40% improved tensile strength with respect to pure Al, whereas an elongation to failure has become of 27.3%, nearly similar to that of cast pure Al [6]. Other than the mechanical property studies, thermal properties were also one of the most important topics in regard to the MMC–CNTs research [7–9].

HPT is one of the severe plastic deformation (SPD) techniques that allows one to achieve very large deformations without heating, under vacuum sintering conditions. Typically, a HPT method has frequently been applied for the grain refinement in bulk coarse-grained metals [10,11], but it is also fully capable of consolidating pure metallic powders [11] or their blends with CNTs [12,13]. Due to a very high applied pressure and imposed shear strain, ultrafine-grained (UFG) or nanocrystalline microstructures are formed in the consolidated samples, even if the initial powders consist of coarse grains. Grain refinement is important for increasing hardness according to the Hall–Petch relationship [14]. For the MMC–CNT works by a HPT method, Al [15–17] and Cu [18–20] were the main metal candidates, similar to SPS studies. For example, Tokunaga

\* Corresponding author at: Nanotube Unit, World Premier International Center for Materials Nanoarchitectonics (WPI-MANA), National Institute for Materials Science, Namiki 1-1, Tsukuba, Ibaraki 3050044, Japan.

E-mail address: [GOLBERG.Dmitri@nims.go.jp](mailto:GOLBERG.Dmitri@nims.go.jp) (D. Golberg).

et al. [15], Joo et al. [16] and Janei et al. [18] analyzed the difference of hardness depending on the area from the center of the HPT samples, because the torsion under high pressure may differently affect the sample center and its edge.

We have been long looking for reinforcing agents other than CNTs for making lightweight and strong Al matrices through a powder metallurgy route. And multi-walled boron nitride nanotubes (BNNTs) have drawn our prime attention [21,22]. These nanotubes possess the crystal geometry identical to those of CNTs (in which each C atom is replaced by alternating B and N atoms), but their properties are totally different. The perfectly straight and peculiar de-bundled appearance of BNNT makes their placement in a given metal matrix more technological compared to CNTs. It is also worth noting that BNNTs are far more chemically and thermally stable compared to CNTs, while having nearly the same huge values of Young's modulus ( $\sim 1$  TPa) and ultimate tensile strength ( $> 30$  GPa) [23].

It is worth mentioning that decent successes have already been achieved by us using BNNTs for improving conventional polymers or ceramics over the past decade [24,25]. By contrast, metal/BNNT composites are almost entirely unstudied materials. Only a few reports globally, including ours, have been published with respect to these new composites. For instance, Singhal et al. [26] while using powder sintering route observed an increase of compressive strength and microhardness of Al/BNNT samples compared to non-doped Al compacts. Agarwal's group has explored the Al/BNNT chemical interfacial reactions [27]. Most recently this group has made an initial attempt to make Al/BNNT composites using a SPS technique [28], i.e., Lahiri et al. stated that BNNT had survived high pressure and temperature over prolonged time needed for SPS. Performed micro-pillar compressive tests showed 50% improvement in both yield and compressive strength with 5.0 vol% BNNT addition into an Al matrix.

But it is important to note that multi-walled BNNTs that Singhal et al. [26] and Lahiri et al. [27,28] utilized in their studies were not of preferred morphologies. They possessed so-called bamboo-like structures formed under a ball milling synthesis [29]. According to our comparative in situ TEM direct tensile tests on individual BN tubes of different morphologies, such nanostructures are several times weaker (having strength below 8 GPa [30]), compared to well crystallized nested and long (up to 10–20  $\mu\text{m}$ ) BN tubular cylinders or polygons routinely produced by us [23].

Over the past two years, using these perfectly shaped and well-structured BNNTs we successfully fabricated various metal–matrix composites made of Al and BNNTs using ion-implantation [31], magnetron sputtering [32] and melt-spinning [33], and analyzed their tensile and bending properties at the nano- and micro-scales. Drastic improvement of the Al mechanical performance was documented on nano- and micro-samples. However, while addressing the issues of future mass production of light and strong MMCs, one essentially needs to move toward the powder metallurgy route which is able to produce macro-samples at high yields.

Therefore, this paper was planned as to fabricate bulky Al–BNNT composites using two selected and efficient compacting procedures, namely, SPS and HPT, and to comparatively analyze structural peculiarities and mechanical properties of the fabricated composites toward their further possible technological implementations.

## 2. Experimental procedure

### 2.1. Powder preparation and consolidation

Multi-walled BNNTs were synthesized by the boron oxide-assisted CVD (BOCVD) method [21,22]. After subsequent high-temperature purification in argon atmosphere, they were dispersed in ethanol using ultrasonic agitator for about an hour. An Al powder (20  $\mu\text{m}$ ,

99.9%, Kojundo Chemicals, Japan) was added into the BNNTs–ethanol solvent and mixed with a stirrer for about 2 h. Ethanol was evaporated after the sample preparation. The starting Al–BNNTs powders were loaded with 1.0–5.0 wt% (i.e.,  $\sim 2$ –9.7 vol%) of BNNTs. The dried powder mixtures were consolidated by SPS ('Dr. Sinter' SPS-511 S apparatus, Sumitomo Coal Mining Co., Japan) in vacuum at 550–600  $^{\circ}\text{C}$  and 50 MPa pressure for 15–20 min in a graphite die, the heating rate was 60  $^{\circ}\text{C}/\text{min}$ . The same Al–BNNT powder mixtures were used for HPT fabrication. The dried powder mixtures were compacted by a REP-HPT-60-05 apparatus, Riken Enterprise Co., Ltd., Japan. Approximately 0.1 g of the powder mixture was put in a circular shallow hole 10 mm in diameter located at the center on the lower anvil of the HPT machine. The lower anvil was lifted to contact the upper anvil as the former was rotated with respect to the upper one at a rotation speed of 1 rpm. Compacting was undertaken at room temperature with an applied pressure of 2.5 GPa. The rotation was initiated 10 s after the load application and terminated after 10 turns. The resultant pellet thickness was  $\sim 0.5$  mm.

### 2.2. Structural analysis

The phase compositions of SPS and HPT compacts were identified by X-ray diffraction (XRD; RINT2000 Ultima III, Rigaku Corporation, Japan) using Cu K $\alpha$  radiation. The morphologies of the polished and fractured surfaces of the samples were investigated by scanning electron microscopy (SEM; S4800, Hitachi Ltd., Japan) and high-resolution transmission electron microscopy (TEM; JEM-2100 F (200 kV), JEM-3000 F (300 kV) and JEM-3100FEF (Omega filter) instruments, JEOL Ltd., Japan). TEM samples were prepared by using focused ion beam (FIB) polishing. Energy dispersive X-ray spectrometry under SEM and TEM investigations (EMAX EX-220, Horiba Ltd., Kyoto, Japan; JEM-3100FEF microscopes) at accelerating voltages of 10 kV (SEM) and 300 kV (TEM), respectively, were employed to identify the composite chemistry and to spatially map the constituting species.

### 2.3. Mechanical property measurements

Microhardness was measured by Vickers indentation using a diamond indenter (Durascan 70, EMCO-TEST Prüfmaschinen GmbH, Austria) under a load of HV0.2 for 10 s. The tensile strength was measured at room temperature on HPT samples by using a tensile test machine (AUTOGRAPH AGS-10KNJ, Shimadzu, Japan) at a strain rate of  $2.0 \times 10^{-3} \text{ s}^{-1}$ . The displacements were measured by a video extensometer with a 3  $\mu\text{m}$  resolution. The samples were cut to 'dog

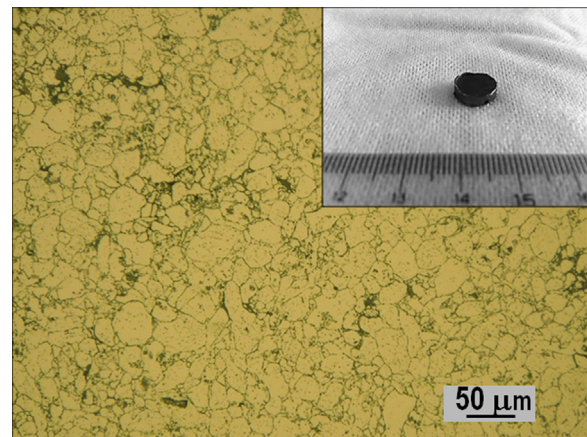


**Fig. 1.** An optical microscopy image of a polished and etched Al-based SPS sample with 1 wt% of BNNT. The average grain size is 10–20  $\mu\text{m}$ . The inset shows the appearance of the actual SPS pellet. It measures around 1 cm in diameter and  $\sim 3$  mm in thickness.

bone' shapes using electrical discharge machining (EDM). All the reported values were the average of at least 4 measurements.

### 3. Results and discussion

#### 3.1. SPS samples

Fig. 1 shows an optical microscopy image taken from an Al–BNNT 1.0 wt% SPS pellet sintered at 550 °C for 20 min after polishing and chemical etching. The Al grain size is about 10–20 μm. The inset displays the real pellet image. Fig. 2 shows XRD spectra of the Al/BNNT

mixed powders before (a) and after SPS (b). The Al phase in both samples is well structured, as evidenced by sharp diffraction peaks coming from the characteristic (111), (200), (220) and (311) reflections. For the mixed powder sample a marginally visible BN (002) peak originated from dispersed BNNTs can be seen at ~26.63° (the inset in Fig. 2 (a)). Those results proved that no other phases, like Al borides or nitrides had been formed in the Al–BNNT composites during mixing and sintering. Fig. 3 displays high-resolution SEM images of an obtained SPS-fabricated Al–BNNT 3.0 wt% composites. The nanotubes are seen being located close to the grain boundaries (Fig. 3c), and sometimes protruding from frequent holes and micropores at the grain boundaries within the samples, Fig. 3a, b and d. HRTEM images

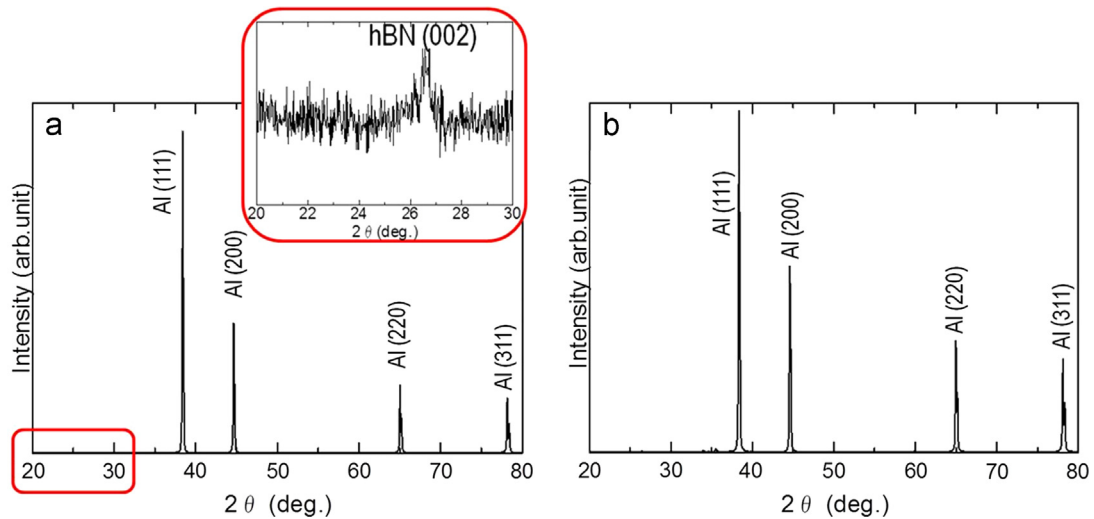


Fig. 2. XRD spectra of the starting powder mixture of Al and BNNT (a) and a SPS-fabricated Al–1wt.% BNNT composite (b). The inset in (a) displays the enlarged range of 20–30° where a characteristic (002) peak of hBN at ~26.5° is visible.

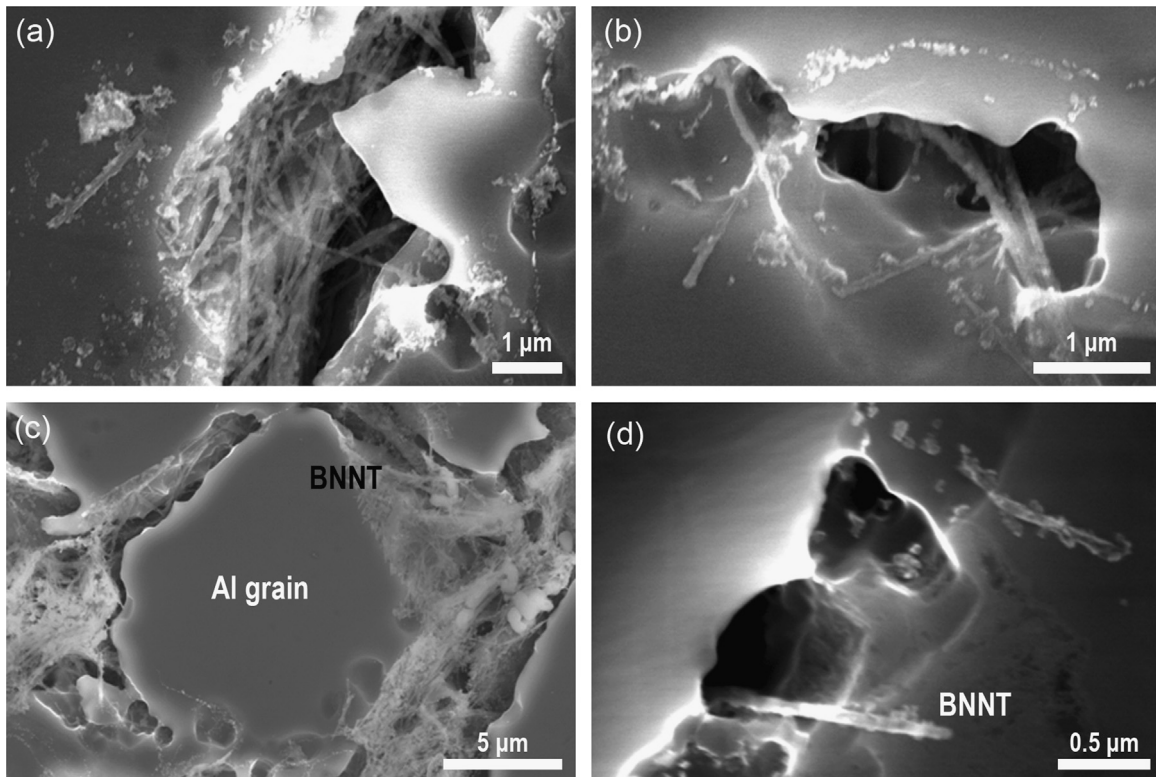


Fig. 3. (a–d) SEM images of a SPS-fabricated Al–BNNT 3 wt% composite. BN nanotubes are seen at the grain boundaries (c); and protruding from microholes at the grain boundaries (a, b and d).

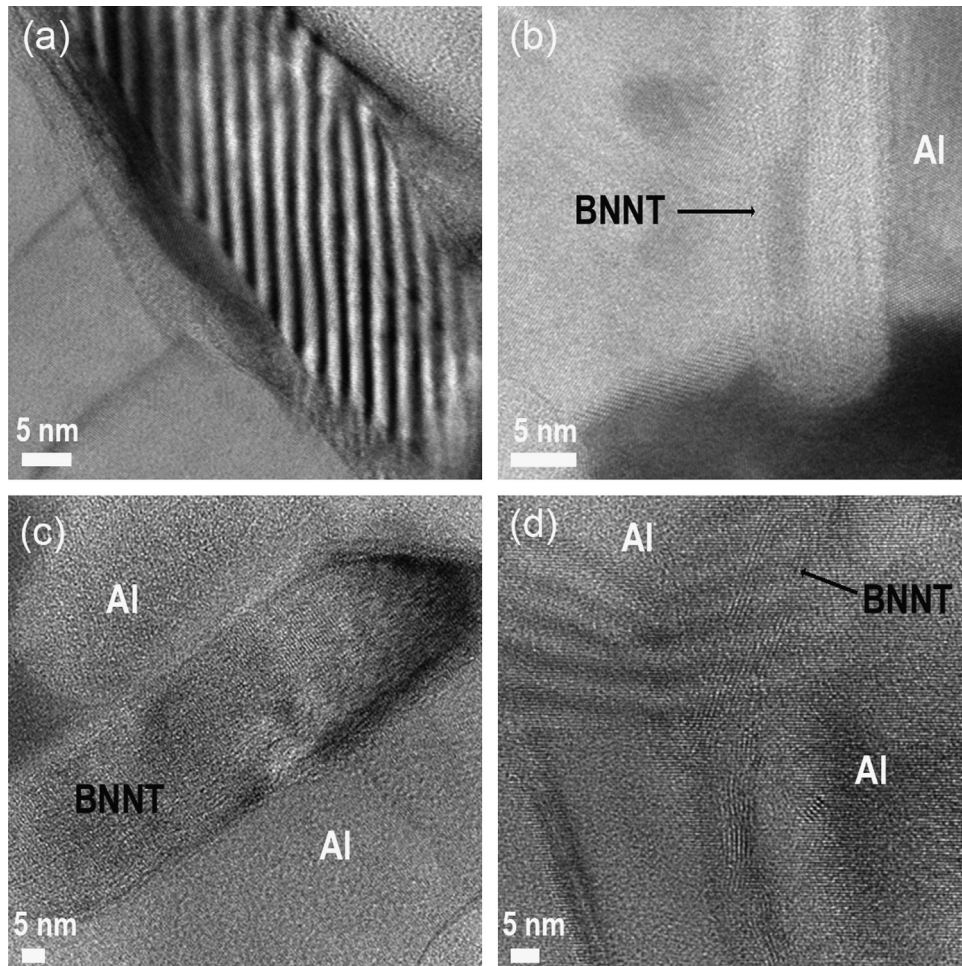


Fig. 4. (a–d) HRTEM images of individual BNNTs located at the vicinity of the Al grain boundaries in a SPS-fabricated Al–BNNT 3 wt% composite.

showing the placements of individual tubes within the structures are depicted in Fig. 4 a–d. The location of an individual nanotube along the grain boundary produces the arresting Moiré contrast (translational+rotational) in Fig. 4a. A shadow-like image of the individual nanotube cap fixed at the grain boundary is visible in Fig. 4b. And individual tube fragments within the Al matrix are seen in Fig. 4c,d. Characteristic (002) fringes separated by a 0.33 nm distance, peculiar to a Van-der-Waals spacing in hBN are particularly visible in Fig. 4d, as marked with an arrow.

Representative room temperature microhardness tests on sintered samples are presented in Fig. 5. The maximal measured hardness of a SPS compact was  $\sim 35$  MPa (for the pure Al). It remains basically unchanged or even slightly decreases with an increased amount of BNNTs in the composites. This means that BNNTs made a little change to the overall Al mechanical properties for the regarded samples. We noticed that Kurita et al. reported that the hardness of the Al–CNT 5 wt% SPS sample was about 35 MPa, the same value as measured here [6]. By contrast, our results notably contradict the recent data by Lahiri et al. [28]. This discrepancy is thought to be due to a notable microporosity of the present SPS samples, e.g., Fig. 3b and d, which cannot be overcome during sintering and spoils the effects of possible reinforcement owing to the strong BN phase. The porosity and related grain boundary discontinuity progresses with an increase of BNNT contents explaining further decline in sample hardness. These embrittlement factors do not allow us to perform proper machining of the decent quality, small sized, dog-bone shaped samples to evaluate the tensile strength of the SPS composites. Fractured surfaces of the SPS composites are illustrated in Fig. 6a and b. Notably, the nanotube and Al phases do not have a strong cohesion to each other. BNNTs are seen

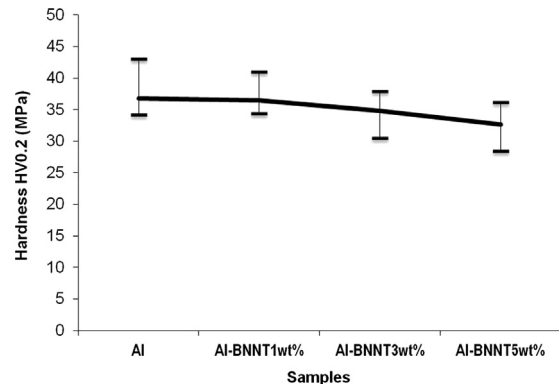
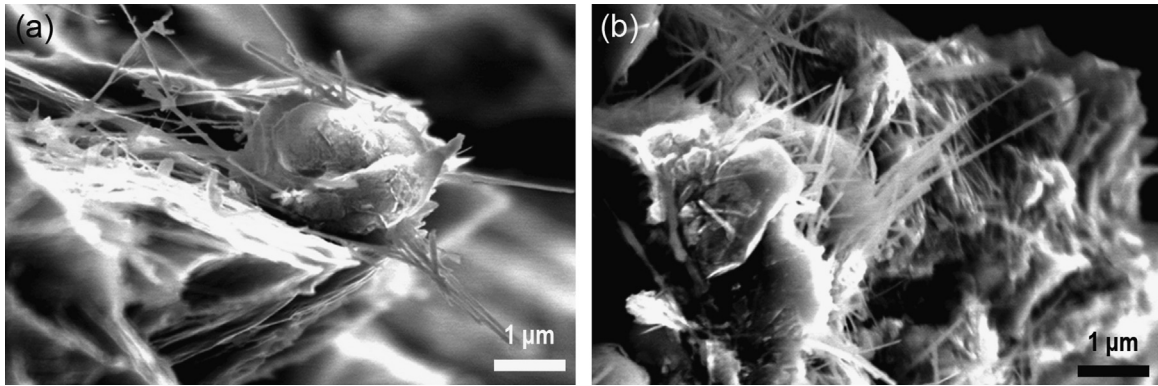


Fig. 5. Hardness of SPS-fabricated Al–BNNT composites as a function of BNNT fraction.

being easily pulled out of the metal matrices, Fig. 6a and b. This tells us that the poor adhesion of BNNTs to metals, and their known nonwettability, that put severe restrictions on an effective load transfer from a soft Al-matrix to the hard BNNT phase, are still the serious existing issues limiting the possibilities of making strong Al–BNNT SPS composites.

### 3.2. HPT samples

Fig. 7 shows comparative XRD spectra of pure Al and Al–BNNT 1.0–3.0 wt% HPT pellets. The same Al–BNNTs mixed powders were used as for the SPS samples. Again, no other phases like Al borides



**Fig. 6.** (a and b) Fracture surfaces of SPS-fabricated Al-BNNT 3 wt% composites. BNNT are seen to be not properly integrated into the Al matrix, being freely protruding from it without decent wetting by the Al body.

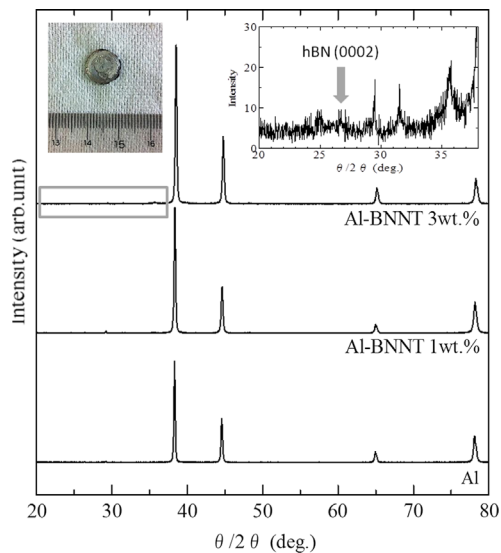


**Fig. 7.** Comparative XRD spectra of HPT-fabricated pure Al and Al-BNNT composites. The right-hand inset in the upper section of the figure displays the enlarged range of 20–38° where a characteristic (002) peak of hBN at  $\sim 26.5^\circ$  is hardly visible. Other peaks in this range originate from a supporting substrate. The left-hand side inset demonstrates the actual appearance of a HPT pellet with 1 wt% of BNNT. It measures around 1 cm in diameter and  $\sim 0.5$  mm in thickness.

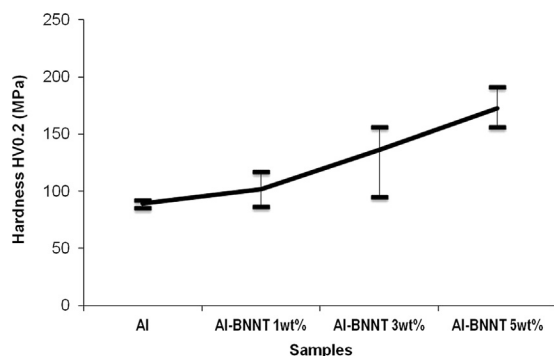


**Fig. 8.** Hardness of HPT-fabricated Al-BNNT composites as a function of BNNT content.

or nitrides form in the well-crystallized HPT Al matrix according to a detailed X-ray analysis. The traces of BNNT on the enlarged XRD spectrum may be seen in the right-hand side inset of Fig. 7. The left-hand side inset in Fig. 7 depicts the real image of a HPT-fabricated Al-BNNT 3 wt% pellet.

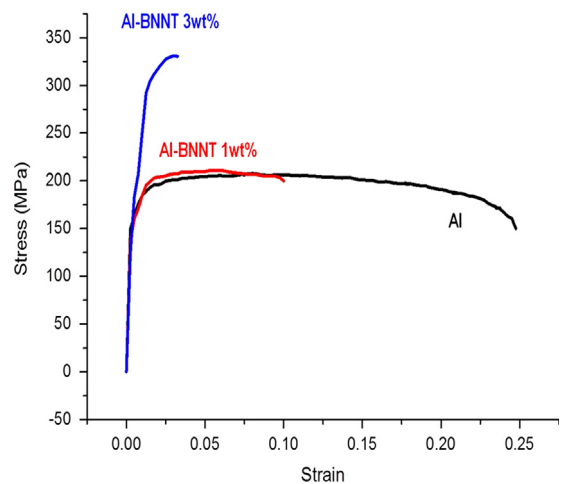


**Fig. 9.** Representative room temperature stress–strain curves of pure Al and Al-BNNT HPT machined composite samples with 1 and 3 wt% of tubes under tension.

**Table 1**  
Summary of HPT-fabricated composite tensile mechanical properties.

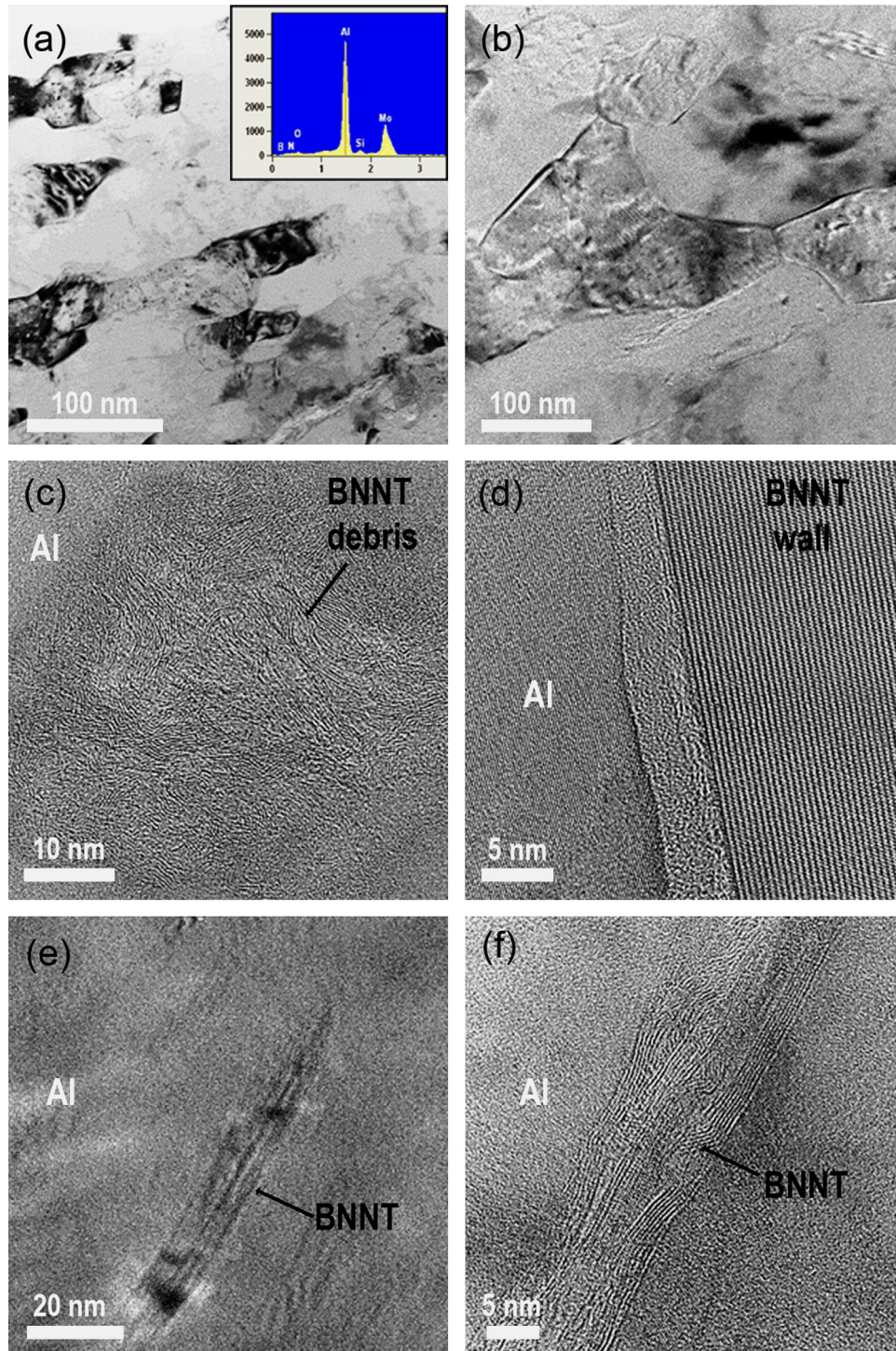
Samples		Fracture strain	Fracture stress (MPa)
Al	1	0.250	207.46
	2	0.218	197.71
	3	0.250	187.29
	4	0.220	202.28
	Ave.	0.239	198.69
BNNT1	5	0.115	206.67
	6	0.075	194.69
	7	0.060	194.86
	8	0.105	210.96
	Ave.	0.089	201.79
BNNT3	9	0.060	264.27
	10	0.053	331.09
	11	0.073	344.47
	12	0.063	278.59
	Ave.	0.062	304.61

Fig. 8 illustrates the micro-Vickers hardness data of pure Al and Al-BNNT HPT-made samples. The hardness increases with increased contents of BNNTs. The hardness of a pure Al sample is  $\sim 90$  MPa, whereas that of an Al-BNNT 5 wt% is  $\sim 190$  MPa, more than a doubled figure. The hardness difference for various HPT

sample areas was also analyzed. Ten to twelve measurements were performed on each pellet face along various imaginary lines drawn in various orientations. On every scan, the hardness value increased with increasing BNNT content compared to pure Al samples.

Representative room temperature stress–strain curves of pure Al sample and those with various BNNT-loading fractions are shown in Fig. 9. The maximum measured strength was close to  $\sim 350$  MPa (Al–BNNT 3.0 wt%) and that of Al–BNNT 1.0 wt% and Al

were around 200 MPa. The curves for Al and Al–BNNT 1.0 wt% samples look nearly similar, as we have seen earlier for the melt-spun composites [32,33], i.e., low BNNT contents are not able to notably modify the composite tensile properties. However, for a 3.0 wt% BNNT sample, the tensile strength is already dramatically increased. The average ultimate tensile strength becomes  $\sim 1.5$  times larger than that of pure Al–HPT compact. Comparing pure Al and Al–BNNT composite samples, the plasticity is also seen to be



**Fig. 10.** Low- (a and b) and high-magnification (c–f) TEM images showing elongated Al grains and appearance of BNNT in HPT composite samples tested in tension (c–f). The inset in (a) depicts an EDX spectrum recorded from the field of view in (a). Smashed (c); well-structured (d), flattened (e) and torn (f) BNNT may be found after the tensile tests of HPT-fabricated samples.

affected. The fracture strain for pure Al is  $\sim 0.24$ , while for an Al–BNNT 1 wt% it becomes  $\sim 0.09$  and for a 3 wt% sample it drops to  $\sim 0.06$ . It could be concluded that the HPT composite samples with nanotubes became much stronger but less ductile with increasing BNNT contents.

Summarized tensile data for 3 sample series are presented in Table 1. The samples with 5 wt% of BNNT were not tested due to their relative brittleness and difficulties in their machining down to small dimensions needed for the microtensile testing machine, see Fig. S1 (Supporting information).

Fig. 10 depicts low- and high-resolution TEM images of the Al–BNNT 3.0 wt% HPT composite samples near their fractured areas after the tensile tests. The clean and slightly elongated Al

nanoscale grains are apparent on the low-magnification image. The enclosed EDX spectrum recorded from the area of view in Fig. 10 a shows weak traces of BN and clear Al and Mo peaks, the latter is coming from a Mo–FIB support used. These data confirm the entire chemical purity of HPT samples used for the tensile tests. Compared to SPS composites the Al grain size is greatly reduced, to several hundred nm. In many cases the nanotube wall structures remain fully preserved, as shown in Fig. 10d after heavy shear deformation during HPT processing. The Al grain and BNNT wall are separated with a sort of an amorphous-like Al layer having a thickness of less than 5 nm in Fig. 10d. In other cases the tube morphology or its wall structures are changed. In Fig. 10c numerous tube walls are seen coagulated in a sort of hBN debris,

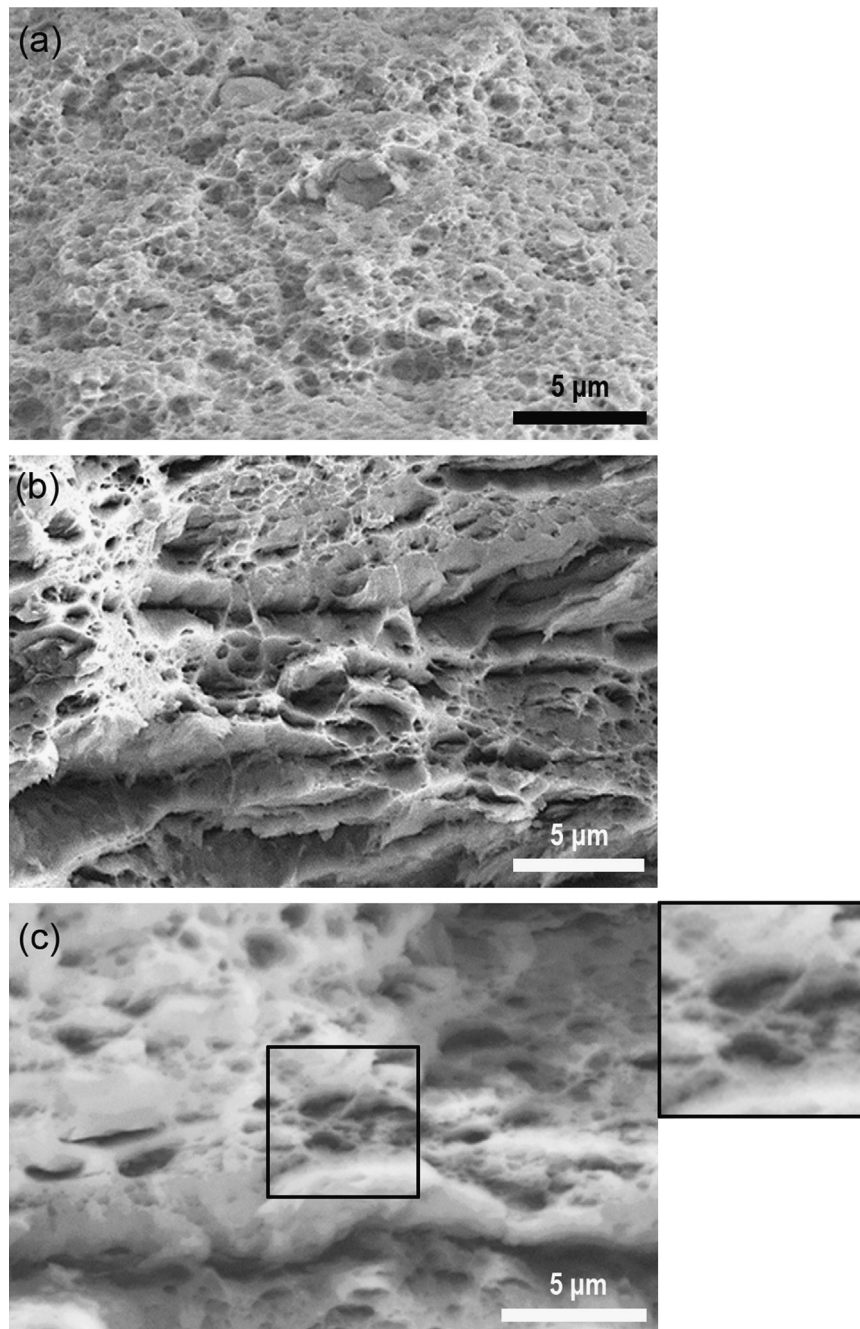


**Fig. 11.** SEM images of the fracture surfaces of tensile tested pure Al (a), Al–BNNT 1 wt% and Al–BNNT 3 wt% HPT composites. The inset in (c) shows the enlarged framed area where three individual BNNTs are seen bridging the two Al bulk portions across the existing micropore.

individual tubes lost their integrity and became bundled and/or jammed. In addition, the individual tube channel may be smashed (Fig. 10e) due to the tube cross-sectional flattening under heavy shear deformations; or the tube may be torn or twisted along its axis, as illustrated in Fig. 10f. Both the existing Al and crystalline *h*BN reflections on numerous electron diffraction patterns, taken from the areas analogous to those shown in Fig. 10c and f confirmed that both phases had kept their individual crystallinity and are not chemically mixed, rather they created rather dense physical mixtures in which the tensile load may decently be transferred from a weaker Al to a stronger BNNT phase.

To judge the differences in the fracture mechanics, the SEM images of fractured pure Al and Al–BNNT 1–3 wt% samples are finally illustrated in Fig. 11. The pure Al–HPT-made sample has a typical dimple-like fracture surface, consistent with a large strain range of a plastic flow, see Fig. 9. More or less similar features are seen at the low loading fraction of BNNT (1 wt%), Fig. 11b, however, the dimpled structure becomes more coarse and the much less developed dimpled network becomes evident. Some traces of transgranular fracture are apparent in Fig. 11b. However, the fracture surfaces of BNNT-containing samples at high BNNT loading fraction (3 wt%) tend to demonstrate a sort of brittle transgranular failure. The image in Fig. 11c depicts that in some parts (as framed and separately shown on the enlarged inset) the nanotubes fully survived after the sample breakage. Three individual BNNTs create a crossed bridge between the two portions of an Al matrix through the existing micropore, thus cementing the whole structure, in accordance with the observed drastic increase in a HPT composite hardness and strength noticed in Figs. 8 and 9, respectively.

The distinct difference between SPS and HPT composite sample performance is suggested to be due to a drastically different grain size and various degrees of microporosity for the two sample series. HPT processing makes much denser composites where the effects of matrix strengthening (due to BNNT effectively incorporated within the grains) prevail over detrimental effects of porosity. Notable grain refinement in HPT samples compared to SPS ones also leads to an overall denser structure with a lesser number of micropores between the sintered Al grains.

#### 4. Conclusions

We fabricated and compared Al–BNNT macrocomposites by using two different methods of powder metallurgy – SPS and HPT, and utilizing various reinforcing multi-walled BNNT fractions (from 1.0 to 5.0 wt%). Scanning and transmission electron microscopy, X-ray diffraction, and energy dispersive X-ray analysis confirmed the desired integration of the two phases into dense and decently compact composites. Based on the detailed structural analysis, HPT samples were found to possess much denser macro-morphologies. No other phases, like Al borides or nitrides, form in the Al–BNNTs macrocomposites of the two series. The BNNTs were mostly embedded along the Al grain boundaries in the SPS samples, while in the HPT samples they were rather evenly distributed within a fine-grained Al matrix (the average grain size was 10–20 μm for SPS samples, whereas only hundreds of nanometers in HPT samples). The hardness of the SPS-made composites was not changed or even slightly decreased with increasing BNNT content. This was governed by the preferential location of BNNT at the grain boundaries, thus creating a structural mismatch between individual Al grains and forming numerous micropores and structural discontinuities along the grain boundaries detrimental for the overall mechanical performance. By contrast, BNNTs were evenly distributed within the Al matrix in the HPT-made Al–BNNT compacts. BNNTs were found to exist both along

the grain boundaries and within Al grains in the latter samples. As a result, the composite hardness was drastically increased with increasing BNNT content in the Al matrices. The value for Al–BNNT 3.0 wt% samples was more than double (190 MPa) compared to pure Al–HPT compacts (90 MPa). Also, the ultimate tensile strength of Al–BNNT samples containing 3.0 wt% BNNT (~300 MPa) became ~1.5 times larger than that of a nanotube-free HPT–Al material (~200 MPa).

#### Acknowledgments

The authors thank the financial support from the ‘Interseed’ Project of the National Institute for Materials Science (NIMS), Grant no. bb063, from the Grant-in-Aid for Scientific Research No. 23310082 (MEXT), from the Grant-in-Aid for Scientific Research on Innovative Area ‘Bulk Nanostructured Metals’, through MEXT, Japan (Contract no. 22102004), and from the World Premier International (WPI) Center for Materials Nanoarchitectonics (MANA) of the National Institute for Materials Science (NIMS). They are particularly grateful to Prof. Y. Sakka (NIMS) for his permission to use a SPS equipment, and to Drs. Y. Bando, M. Mitome, and N. Kawamoto for valuable discussions. D.G. also acknowledges a ‘Mega-Grant’ award for leading scientists tenable at the National University of Science and Technology ‘MISIS’, Moscow, Russian Federation, under the Agreement no. 11. G34.31.0061.

#### Appendix. Supporting information

Supplementary data associated with this article can be found in the online version at <http://dx.doi.org/10.1016/j.msea.2014.02.086>.

#### References

- [1] S.R. Bakshi, D. Lahiri, A. Agarwal, *Int. Mater. Rev.* 55 (2010) 41–64.
- [2] K.T. Kim, S.I. Cha, S.H. Hong, S.H. Hong, *Mater. Sci. Eng. A* 430 (2006) 27–33.
- [3] S.I. Cha, K.T. Kim, S.N. Arshad, C.B. Mo, S.H. Hong, *Adv. Mater.* 17 (2005) 1377–1381.
- [4] K. Sairam, J.K. Sonber, T.S.R.Ch. Murthy, C. Subramanian, R.K. Fotedar, P. Nanekar, R.C. Hubli, *Int. J. Refract. Met. Hard Mater.* 35 (2014) 185–192.
- [5] H. Kwon, M. Estili, K. Takagi, T. Miyazaki, A. Kawasaki, *Carbon* 47 (2009) 570–577.
- [6] H. Kurita, H. Kwon, M. Estili, A. Kawasaki, *Mater. Trans.* 52 (2011) 1960–1965.
- [7] S.R. Bakshi, R.R. Patel, A. Agarwal, *Comput. Mater. Sci.* 50 (2010) 419–428.
- [8] S. Cho, K. Kikuchi, T. Miyazaki, K. Takagi, A. Kawasaki, T. Tsukada, *Scr. Mater.* 63 (2010) 375–378.
- [9] S. Cho, K. Kikuchi, A. Kawasaki, *Acta Mater.* 60 (2012) 726–736.
- [10] R.Z. Valiev, T.G. Langdon, *Prog. Mater. Sci.* 51 (2006) 881–981.
- [11] A.P. Zhilyaev, T.G. Langdon, *Prog. Mater. Sci.* 53 (2008) 893–979.
- [12] H.J. Choi, J.H. Shin, B.H. Min, J.S. Park, D.H. Bae, *J. Mater. Res.* 24 (2009) 2610–2616.
- [13] H. Li, A. Misra, Y. Zhu, Z. Horita, C.C. Koch, T.G. Holesinger, *Mater. Sci. Eng. A* 523 (2009) 60–64.
- [14] N. Hansen, *Scr. Mater.* 51 (2004) 801–806.
- [15] T. Tokunaga, K. Kaneko, Z. Horita, *Mater. Sci. Eng. A* 490 (2008) 300–304.
- [16] S.H. Joo, S.C. Yoon, C.S. Lee, D.H. Nam, S.H. Hong, H.S. Kim, *J. Mater. Sci.* 45 (2010) 4652–4658.
- [17] H.J. Choi, G.B. Kwon, G.Y. Lee, D.H. Bae, *Scr. Mater.* 59 (2008) 360–363.
- [18] P. Janei, E.Y. Yoon, J. Gubicza, H.S. Kim, J.L. Lábár, T. Ungár, *Mater. Sci. Eng. A* 528 (2001) 4690–4695.
- [19] P. Janei, E.Y. Yoon, J. Gubicza, H.S. Kim, J.L. Lábár, T. Ungár, *Mater. Sci. Forum.* 729 (2013) 228–233.
- [20] P. Janei, J. Gubicza, E.Y. Yoon, H.S. Kim, J.L. Lábár, *Composite A* 51 (2013) 71–79.
- [21] D. Golberg, Y. Bando, C. Tang, C.Y. Zhi, *Adv. Mater.* 19 (2007) 2413–2432.
- [22] D. Golberg, Y. Bando, Y. Huang, T. Terao, M. Mitome, C.C. Tang, C.Y. Zhi, *ACS Nano* 4 (2010) 2979–2993.
- [23] X.L. Wei, M.S. Wang, Y. Bando, D. Golberg, *Adv. Mater.* 22 (2010) 4895–4899.
- [24] C.Y. Zhi, Y. Bando, T. Terao, C.C. Tang, H. Kuwahara, D. Golberg, *Adv. Funct. Mater.* 19 (2009) 1857–1862.
- [25] Q. Huang, Y. Bando, X. Xu, T. Nishimura, C.Y. Zhi, C.C. Tang, F.F. Xu, L. Gao, D. Golberg, *Nanotechnology* 18 (2007) (485706–1–7).
- [26] S.K. Singhal, A.K. Srivastava, R. Pasricha, R.B. Mathur, *J. Nanosci. Nanotechnol.* 11 (2011) 5179–5186.

- [27] D. Lahiri, V. Singh, L.H. Li, T. Xing, S. Seal, Y. Chen, A. Agarwal, J. Mater. Res. 27 (2012) 2760–2770.
- [28] D. Lahiri, V.A. Hadjikhani, C. Zhang, T. Xing, L.H. Li, Y. Chen, A. Agarwal, Mater. Sci. Eng. A 574 (2013) 149–156.
- [29] Y. Chen, J. Zou, S.J. Cambell, G. Le, Appl. Phys. Lett. 84 (2004) 2430–2432.
- [30] D.M. Tang, C.L. Ren, X.L. Wei, M.S. Wang, C. Liu, Y. Bando, D. Golberg, ACS Nano 5 (2011) 7362–7368.
- [31] E.A. Obrastsova, D.V. Shtansky, A.N. Sheveyko, M. Yamaguchi, A.M. Kovaskii, D. Golberg, Scr. Mater. 67 (2012) 507–510.
- [32] M. Yamaguchi, D.M. Tang, C.Y. Zhi, Y. Bando, D.V. Shtansky, D. Golberg, Acta Mater. 60 (2012) 6213–6222.
- [33] M. Yamaguchi, J. Bernhardt, K. Faerstein, D.V. Shtansky, Y. Bando, I.S. Golovin, H.R. Sinning, D. Golberg, Acta Mater. 61 (2013) 7604–7615.